Available online at www.sciencedirect.com

ScienceDirect

Energy Procedia 38 (2013) 872 – 880

Energy Procedia

SiliconPV: March 25-27, 2013, Hamelin, Germany

Al_2O_3 passivation on *c*-Si surfaces for low temperature solar cell applications

Desislava S. Saynova[a]*, Gaby J.M. Janssen[a], Antonius R. Burgers[a], Agnes A. Mewe[a], Elena Cianci[b], Gabriele Seguini[b], Michele Perego[b]

[a]*ECN, Westerduinweg 3, NL-1755 LE Petten, the Netherlands*
[b]*Laboratorio MDM, IMM-CNR, Via C. Olivetti 2,I-20864 Agrate Brianza (MB), Italy*

Abstract

Functional passivation of high resistivity p-type *c*-Si wafer surfaces was achieved using 10 nm Al_2O_3 layers and low temperatures for both the thermal ALD process and post-deposition anneal. Effective lifetime values higher than 1 ms were measured at excess carrier density Δn=10^{15} cm^{-3}. This result was reached in combination with temperatures of 100 °C and 200 °C for the Al_2O_3 layer deposition and anneal, respectively. The Al_2O_3/*c*-Si interface was characterized using conductance-voltage and capacitance-voltage measurements. In particular, significantly reduced interface density of the electrically active defects D_{it} ~ 2 x 10^{10} $eV^{-1}cm^{-2}$ was detected, which enabled excellent chemical passivation. The measured density of fixed charges at the interface, Q_f, after anneal were in the range +1 x 10^{12} to -1 x 10^{12} cm^{-2} indicating that both inversion and accumulation conditions result in relevant field-effect passivation using Al_2O_3 layers and low temperature processes. Numerical simulations on representative test structures show that the uniform Q_f effect can be understood in terms of a surface damage region (SDR) present near the interface in combination with asymmetry in the lifetime of holes and electrons in the SDR. The combination of low processing temperatures, thin layers and good passivation properties facilitate a technology for future low temperature solar cell applications.

Selection and/or peer-review under responsibility of the scientific committee of the SiliconPV 2013 conference

Keywords: Al_2O_3 ALD layers; low temperature processing; interface passivation; numerical simulation; surface damage region

* Corresponding author. Tel.: +31 88 515 4093; fax: +31 88 515 8214.
E-mail address: saynova@ecn.nl.

1876-6102
Selection and/or peer-review under responsibility of the scientific committee of the SiliconPV 2013 conference
doi:10.1016/j.egypro.2013.07.359

1. Introduction

Passivation schemes utilizing Al_2O_3 ALD layers have demonstrated high performance levels on both p- and n-type *c*-Si surfaces of suitable doping levels for high efficiency solar cells [1, 2]. The key factor in this respect is the combination of chemical passivation enabled by low interface state defect density (D_{it}), typically 1×10^{11} $eV^{-1}cm^{-2}$ and field-effect passivation due to a large amount of fixed negative charges (Q_f) in the range of $(2 – 6) \times 10^{12}$ cm^{-2} located at the Al_2O_3/*c*-Si interface [3-5]. Both D_{it} and Q_f can be significantly influenced by the type of ALD, oxygen precursor, post-deposition anneal (PDA) step and film thickness [6, 7]. Thermal ALD (T-ALD) using H_2O as oxygen precursor represents a particularly suitable method for low temperature applications. In particular, comparisons with plasma ALD or T-ALD with O_3 show that in as-deposited state typically at 200 °C the D_{it} values using thermal ALD with H_2O are lower by two orders of magnitude. As a result the passivation at that stage is better for the latter approach, even though the corresponding Q_f values are reduced by a factor of 10 [3] compared to the other two methods. This trend is also reported for PDA temperatures up to 350 °C applied for 10 min [6]. In spite of the demonstrated impressive surface passivation results with effective recombination velocities $\leq$ 5 cm/s the processing conditions are not suitable for low-temperature solar cell technologies, such as silicon heterojunction technologies. With respect to thickness, Al_2O_3 layers deposited by thermal ALD with H_2O below 10 nm result in a rapid lifetime decrease from about 1ms to only a few tens of µs [6-8]. The effect is attributed to reduced chemical passivation and demonstrates the performance sensitivity towards the passivation scheme design.

This paper presents an investigation of the passivation on high resistivity p-type *c*-Si wafer surfaces by Al_2O_3 layers with thickness of 10 nm and our focus is on low temperature processes for both thermal ALD and PDA. The characterization comprises effective lifetime measurements on symmetrical samples as well as D_{it} and Q_f evaluation using metal-oxide-semiconductor capacitors. In addition, numerical simulations on representative test structures have been carried out. The results are compared with the experimental data in order to gain a better understanding of the physical mechanism of the passivation performance and identify further improvement options for the performance of the Al_2O_3 layers in low temperature solar cell applications.

Nomenclature

Q_f	fixed charges at the dielectric layer/*c*-Si interface
D_{it}	interface state defect density
τ_{eff}	effective lifetime measured using photo-conductance method
Δn	excess carrier density in the quasi-neutral region (bulk) of the silicon wafer
$S_{eff\,MAX}$	maximum surface recombination velocity assuming infinite bulk lifetime, $S_{eff} \leq W/2\,\tau_{eff}$
W	wafer thickness
N_{acc}	dopant concentration of p-type silicon wafer
S_p, S_n	surface recombination velocity for holes and electrons, respectively. $S_p=\sigma_p v_{th} N_{it}$ and $S_n=\sigma_n v_{th} N_{it}$.
$\tau_{s,p}$, $\tau_{s,p}$	life-time of holes and electrons in the surface damage region
$\tau_{0,p}$, $\tau_{0,p}$	life-time of holes and electrons
$\sigma_{p,}$ σ_n	capture cross section at the interface of holes and electrons, respectively

N_{it}	interface defect density
v_{th}	thermal velocity of of the charge carriers (10^7 cm s^{-1})
p_s, n_s	hole and electron concentration at the surface, respectively
p_1, n_1	density of defects at midgap
S_{eff}	effective surface recombination velocity
$n_{i,eff}$	effective intrinsic charge carrier density

2. Al_2O_3/*c*-Si interface - electrical characterization and passivation results

2.1. Experimental details and characterization methods

The 10-nm-thick Al_2O_3 films were obtained by thermal ALD using $Al(CH_3)_3$, trimethyl-aluminum (TMA), and H_2O as precursors at T_{ALD} ranging between 100 °C and 200 °C. The TMA and H_2O exposure times were 0.015 s, the N_2 purge time following both reactant exposures was 8 s. The growth per cycle at 100 °C was 1.0 Å/cycle, increasing to 1.1 Å/cycle at 150-200 °C. After the ALD process the films were subjected to a heat treatment in a rapid thermal anneal (RTA) furnace for 5 min in N_2 atmosphere. The corresponding temperatures for this step were T_{PDA} of 200 °C or 250 °C. Al_2O_3 films were deposited simultaneously on both sides of H-terminated double-side polished p-type float zone FZ<100> Si wafers (resistivity 2-4 Ω cm, thickness 280 ± 25 μm). This deposition scheme allows avoiding any difference between the two *c*-Si/Al_2O_3 interfaces. The film thickness was measured by spectroscopic ellipsometry.

The H-terminated Si (100) surfaces were obtained by means of standard cleaning in a $HCl:H_2O_2:H_2O$=1:1:5 solution for 10 min at 85 °C followed by a 30 s dip in diluted HF ($HF:H_2O$=1:50) at room temperature.

Dedicated single sided deposition processes on H-terminated single-side polished p- and n- type *c*-Si were performed to fabricate the metal-oxide-semiconductor (MOS) capacitors for electrical characterization of the Al_2O_3/*c*-Si interface and evaluation of Q_f and D_{it}. The metallization of the MOS structures was obtained by evaporation technique. The front side coated with Al_2O_3 was contacted via Al dots of 0.08 mm^2 area patterned using a shadow mask. Full Al layer deposition was applied to the opposite side. Capacitance-voltage (CV) and conductance-voltage (GV) measurements were acquired simultaneously at 100 kHz in a dark environment in a shielded probe station at room temperature. The measurements were performed from inversion to accumulation and vice versa to check the presence of hysteresis loops in the CV characteristics. Series resistance correction was applied to all measurements before the CV and GV data analysis [9].

The functionality of the surface passivation using Al_2O_3 layers was monitored by effective lifetime (τ_{eff}) measurements on double side-coated samples as a function of the excess carrier density (Δn) using a WCT-120: Silicon Wafer Lifetime Tester from Sinton Instruments in transient or quasi-steady state mode [10].

2.2. Experimental results and discussion

An overview of the passivation by Al_2O_3 films monitored using effective lifetime measurements and the interface properties characterized via Q_f and D_{it} evaluation is shown in Fig. 1. The reported lifetime results are averaged within each group with error bars representing the standard deviation. An experiment

group contained 2 samples. The result for each sample was averaged over 5 measurements. The plot data for Q_f and D_{it} are the average values from two different sweep directions: from inversion to accumulation and vice versa. The CV and GV measurements were of high reproducibility with essentially the same results for several capacitors and error bars comparable to the size of the symbols in the graph of Fig. 1.

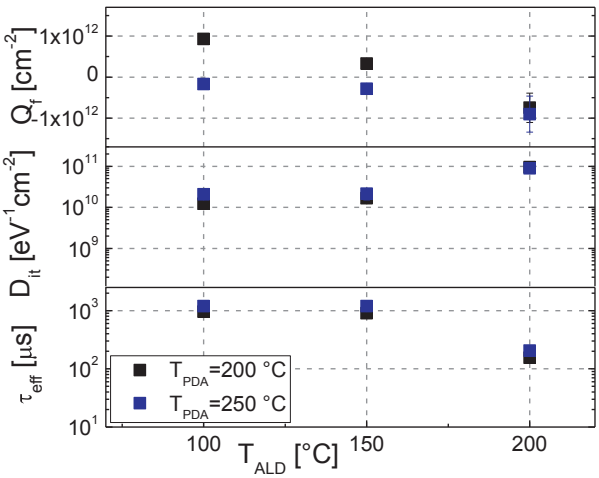

Fig. 1 Plot of the variation with the deposition temperature T_{ALD} of effective lifetime values, interface defect density D_{it} and the fixed charge Q_f. The results shown are for two different anneal temperatures T_{PDA}

The results show that the temperatures used for both ALD and PDA processes have an influence on the passivation performance of the Al_2O_3 films and the characteristics of Al_2O_3/*c*-Si interface. However, the higher impact was found for the ALD conditions. Effective lifetimes $\geq$ 1 ms have been achieved even for the lowest deposition temperature of 100 °C. PDA at 250 °C shows higher and more stable results compared to 200 °C with (1.2$\pm$0.02) ms vs. (1$\pm$0.15) ms, respectively. Those values are comparable to other reports about thermal ALD Al_2O_3 layers of 10 nm applied for passivation of (100) p-FZ wafers in the resistivity range 1.5 – 2.5 Ohm.cm [6, 7]. Nevertheless, in our case the temperatures for sample preparation were significantly reduced, both in terms of deposition (200 °C mentioned in the reports) and anneal (reference range between 350 °C and 425 °C for 10 – 15 min). In this way the overall process conditions for the Al_2O_3 passivation layers in the current study are compatible with low-temperature solar cell technologies. The corresponding D_{it} values after anneal are 1-2 × 10^{10} $eV^{-1}cm^{-2}$ and significantly lower than the literature reports of 4 – 10 × 10^{10} $eV^{-1}cm^{-2}$. The chemical passivation is the most sensitive factor when the film thickness of the ALD Al_2O_3 is considered [5, 7]. Higher T_{ALD} of 200 °C substantially reduced the effective lifetime to ~200 μs for both anneal temperatures. Simultaneously D_{it} increased to 1 × 10^{11} $eV^{-1}cm^{-2}$. In this way the passivation was at the lowest level, although Q_f, as discussed in more details below, reached the highest negative values of (1 $\pm$ 0.4) × 10^{12} cm^{-2}. This result suggests that D_{it} values below 1 × 10^{11} $eV^{-1}cm^{-2}$ are needed for the achievement of high lifetime values and the interface optimization is essential for further improvement of the low temperature passivation employing thin Al_2O_3 layers. Concerning the field effect passivation, increasing the PDA temperature from 200 °C to 250 °C the sign of Q_f changed from positive to negative for both deposition temperatures of 100 °C and 150 °C. In case of ALD process at 200 °C the resultant Q_f was already negative and the anneal did not have a significant additional impact. The best negative Q_f of (1 $\pm$ 0.4) × 10^{12} cm^{-2} was in the lower range of the typical literature data ~(1 – 4) × 10^{12} cm^{-2}. However, higher anneal temperatures have been employed for the quoted examples. The exact mechanism of the impact on Q_f of the thermal treatment is not fully clarified at present and needs further investigation of the chemical and structural properties of the

Al_2O_3/*c*-Si interface. In particular, the cause for the change of the Q_f sign from positive to negative for the samples with $T_{ALD} \leq 150$ °C and $T_{PDA} = 250$ °C can be identified by performing a depth resolved element composition quantification of the Al_2O_3 layers. Earlier reports show that Al-rich configurations with high amount of Al_i yield positive Q_f, whereas negative Q_f values correspond to O-rich structures with enhanced O_i and Al vacancies [7, 11-13]. Electron energy-loss spectroscopy can also be applied to investigate Al energy-loss near-edge structures (ELNESs) and extract information about tetrahedrally and octrahedrally coordinated Al atoms in the Al_2O_3 films [14]. The first bonding environment for Al corresponds to a negative charge while in the latter case the charge is positive [15, 16]. Another important factor influencing the Q_f in case of Al_2O_3 layers is the interface SiO_x which can be monitored using high resolution transmission electron microscopy images (HR TEM) [7, 17, 18]. In the present study we measured effective lifetime values ≥ 1 ms at deposition temperatures below 200 °C for both positive and negative Q_f. The best passivation in terms of lifetime values ~ 1.2 ms and low spread of the results was achieved for negative Q_f and accumulation conditions.

The observation that at deposition temperatures lower than 200 °C the measured lifetime values are not strongly dependent on the sign and magnitude of the Q_f, requires further investigation. The total impact of Q_f depends also on the density of the interface states and on the lifetime of the charge carriers in the wafer region close to the interface. With respect to the latter contribution it has been proposed in the literature [19, 20] that application of passivation layers may result in a so-called surface damage region (SDR) where the charge carrier lifetime is significantly lower than in the bulk of the wafer. In the next section numerical simulations are presented that include effects at the interface and in the SDR to explain why Q_f with different sign and magnitude can have a similar impact on the passivation.

3. Numerical simulations

3.1. Approach

The modeling of the passivation properties of the Al_2O_3 layers on *c*-Si surface is based on the well-known Shockley-Read-Hall formalism [21, 22]. The recombination at the interface is then written as:

$$R_{it} = \frac{p_s \cdot n_s - n_{i,eff}^2}{(1/S_p)(n_s + n_1) + (1/S_n)(p_s + p_1)} \quad (1)$$

The parameters S_p and S_n characterize the recombination at the interface defects. The charge density Q_f will have a large impact on n_s and p_s. On p-type *c*-Si negative Q_f will induce accumulation of holes at the interface, and positive charges will induce either depletion of the holes or even inversion conditions where $n_s > p_s$.

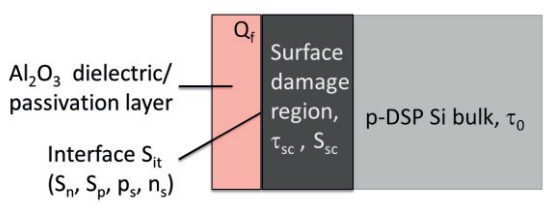

Fig. 2 Representative test structure used for the numerical simulations

The effect on the carrier concentrations in is not limited to the interface but comprises a whole space charge region (SCR), the depth of which depends on the dopant concentration of the *c*-Si. For doped *c*-Si wafers SCR is typically less than 1 µm. As explained at the end of the previous section, in a SDR the lifetimes are reduced as compared to the bulk. Therefore, this region can contribute substantially the total recombination, and the contribution will depend on the sign and magnitude of Q_f [19, 23]. The recombination rate in the SDR is written at each point z (representing the distance to the interface) as:

$$R_{SDR}(z) = \frac{p(z)\cdot n(z) - n_{i,eff}^2}{\tau_{s,p}(n(z)+n_1)+\tau_{s,n}(p(z)+p_1)} \quad (2)$$

with $\tau_{s,p}$ and $\tau_{s,n}$ being the hole and electron lifetimes in the SDR and n_1 and p_1 defined as before. The passivating effect of Q_f can be characterized by S_{eff}, which is defined by:

$$S_{eff}\,\Delta n = R_{it}(n_s, p_s, S_n, S_p) + \int R_{SDR}(n(z), p(z)\ \tau_{s,n}, \tau_{s,p})dz \quad (3)$$

with Δn being the excess carrier density directly outside the surface damage region.

Numerical simulations using the Atlas software from Silvaco [24] have been carried out to investigate the relative contributions to S_{eff} for various Q_f values. A representative test structure depicted in Fig. 2 was used. In the simulations the structure is illuminated by a monochromatic light with λ=500 nm.

The acceptor concentration in *c*-Si was fixed at $5\cdot10^{15}$ cm^{-3} corresponding to a resistivity of 2.8 Ohm cm. The SDR region had a width of 300 nm which at this resistivity is large enough to contain the space charge region. It was assumed that the lifetimes are constant over the whole SDR, i.e. in the simulations the lifetime of electrons and holes is a step function with a step at 300 nm from the interface. The effective lifetime in the SDR was adapted to the experimental results (see below). For the bulk lifetimes $\tau_{0,p} = \tau_{0,n} = 2$ ms were assumed.

3.2. Simulation results and discussion

The experimental data considered for the numerical simulations correspond to Al_2O_3 deposition temperatures at 100 °C and 150 °C. The selection is suitable for understanding the effect of variations in the field effect passivation, because the Q_f values change from positive to negative depending on the anneal conditions. At the same time D_{it} remained comparable in the range of 1-2 x 10^{10} eV^{-1}cm^{-2} providing for a high level of chemical passivation. Experimental results for the maximum surface recombination velocity $S_{eff\,MAX}$ as function of the excess density are displayed in Figure 3a. The $S_{eff\,MAX}$ was calculated from the measured effective lifetime values and assuming infinite bulk lifetime. The corresponding Q_f values are also included.

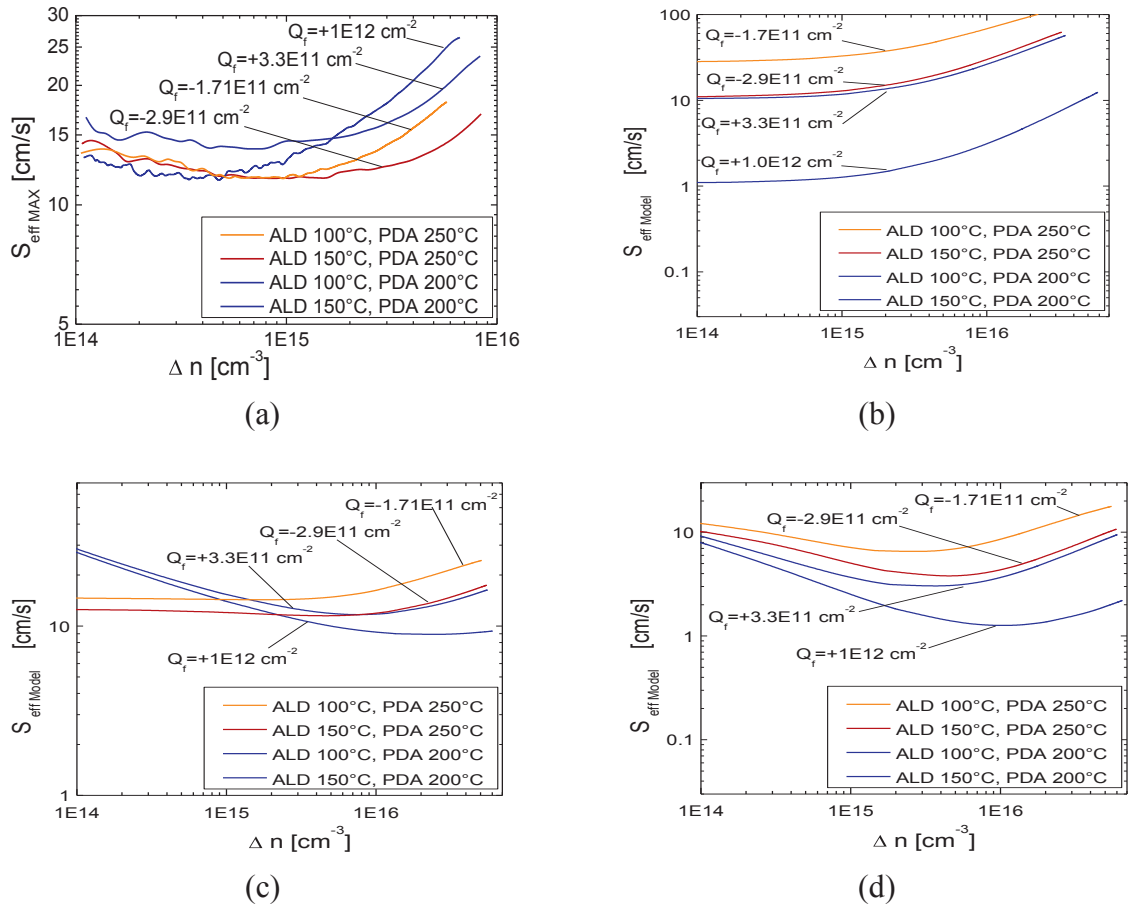

Fig. 3 (a) Experimental results for the maximum surface recombination velocity ($S_{eff\,MAX}$) vs. excess carrier lifetime, (b) calculated S_{eff} vs. excess carrier lifetime without SDR, (c) numerical simulation results for S_{eff} vs. excess carrier lifetime including SDR and assuming similar lifetime values for electrons and holes, (d) model results for S_{eff} vs. excess carrier lifetime including SDR and difference by a factor of 20 in lifetime values for electrons and holes

The results of simulations without a SDR (i.e. $\tau_{s,p} = \tau_{s,n} = 2$ ms) are shown in Fig. 3b. The limiting values in Fig. 3b at low injection are consistent with using $S_p = S_n = 600$ cm s^{-1}. These values were selected such that the average value of the calculated S_{eff} is in the same order of magnitude as the experimental values in Fig. 3a. Although Fig. 3b shows that Q_f with similar magnitude but opposite sign can result in the same passivation, this approach overestimates the dependence on the magnitude of Q_f.

Fig 3c shows the calculated S_{eff} when it is assumed that both the SDR and the interface contribute to the recombination. Compared to Fig. 3b the interface contribution (Eq. 1) is now reduced. i.e. $S_p = S_n = 60$ cm s^{-1}, and the SDR is modeled with $\tau_{s,p} = \tau_{s,n} = 2$ µs. A good agreement could be obtained between the calculated and experimental data for the two negative charges, i.e. the cases where accumulation occurs and $\tau_{s,n}$ determines the recombination (Fig. 3c) The positive charges induce inversion conditions and this can result in high recombination rates in the SDR especially at low injection conditions (Fig. 3c). However, the latter effect is not prominent in the experimental results (comparison between Fig. 3a and Fig. 3c). The effect of inversion conditions is mitigated by assuming $\tau_{s,p} > \tau_{s,n}$. Fig. 3d shows the results of

simulations using $S_p = S_n = 60$ cm s^{-1}, $\tau_{s,n} = 2$ µs and $\tau_{s,p} = 40$ µs. Comparison of Fig. 3a and Fig. 3d shows that with the assumptions made above the both the order of magnitude of S_{eff} as well as the relatively weak dependence on the sign and magnitude of Q_f can be explained.

The assumptions made here are consistent with both the results for the D_{it} discussed above and with data from the literature. When it is assumed that the electrically active interface defects yielding the experimentally obtained D_{it} are the main source for contribution to N_{it}, the resultant values for the electron and hole capture cross sections are in the order of 6×10^{-16} cm^2. This is in excellent agreement with values reported by Werner et al. for Al_2O_3/*c*-Si interfaces [20]. As mentioned earlier, the presence of a SDR was proposed by Steingrube et al.[19] to explain the passivation properties of SiN_x/*c*-Si interfaces and also used to by Werner et al. to describe the passivation at Al_2O_3/*c*-Si interfaces. In both papers an asymmetry $\tau_{s,p} > \tau_{s,n}$ was assumed which was further corroborated by capture cross section measurements of Werner et al. at interface defects. It should be noted that the type of samples in our study comprising high resistivity p-type *c*-Si DSP wafers may facilitate higher performance sensitivity towards SDR-related effects.

An independent characterization of the SDR region is not yet available, i.e. it has not been established which type of damage has been incurred during the processing of the wafer. A tentative explanation for the presence of an SDR by Steingrube et al. is based on experimental observations that during layer deposition or during the preceding etching step hydrogen is introduced into the *c*-Si. High concentrations of hydrogen may then form active recombination centers. The simulation results suggest that reduction of the damage, leading to increased lifetime in the SDR while keeping the interface N_{it} at sufficiently low level, would further improve the passivation properties.

4. Summary and conclusions

A high level of passivation of Al_2O_3/*c*-Si corresponding to $\tau_{eff} \sim 1$ ms was achieved at low temperatures for both ALD and PDA processes ($T \leq 200$ °C). The passivation mechanism was characterized based on D_{it} and Q_f evaluation from CV and CG measurements and numerical simulations on representative test structures. The passivation performance of Al_2O_3 layers in our study was dominated by the deposition temperature rather than PDA conditions. A similar trend was found for the measured electrically active D_{it}. This is an indication of the significant impact of the chemical passivation in case of low temperature process conditions. A considerably lower influence was found for the sign and magnitude of Q_f and thereby the field effect part of the interface passivation. Numerical simulations show that the latter result cannot be understood from the recombination properties at the interface alone. The computation results strongly suggest that there is a substantial contribution from a surface damage region near the interface. This SDR is characterized by a reduced lifetime of holes and electrons, with a stronger reduction for electrons than for holes. These findings are consistent with recent literature reports. Based on the combined experimental and simulation results further improvement options were identified such as reduced layer thickness and dedicated interface optimization in order to facilitate future applications in low temperature solar cells.

Acknowledgements

This work was supported by the EU via project NanoPV (FP7-NMP3-SL-2011-246331).

Arthur Weeber (ECN), Federico Ferrarese Lupi and Jacopo Frascaroli (MDM, IMM-CNR) are gratefully acknowledged for the fruitful discussions. Esther Cobussen-Pool (ECN) and Mario Alia (MDM, IMM-CNR) are gratefully acknowledged for the technical assistance.

References

[1] J. Benick, B. Hoex, M. C. M. van de Sanden, W. M. M. Kessels, O. Schultz, S. W. Glunz, Applied Physics Letters 2008, 92, 53504.

[2] J. Schmidt, A. Merkle, R. Brendel, B. Hoex, M. C. M. van de Sanden, W. M. M. Kessels, Progress in Photovoltaics 2008, 16, 461.

[3] G. Dingemans, N. M. Terlinden, D. Pierreux, H. B. Profijt, M. C. M. van de Sanden, W. M. M. Kessels, Electrochemical and Solid State Letters 2011, 14, H1-H4.

[4] B. Hoex, S. B. S. Heil, E. Langereis, M. C. M. van de Sanden, W. M. M. Kessels, Applied Physics Letters 2006, 89, 42112.

[5] N. M. Terlinden, G. Dingemans, M. C. M. V. de Sanden, W. M. M. Kesselsa, Applied Physics Letters 2010, 96, 12101.

[6] G. Dingemans, R. Seguin, P. Engelhart, M. C. M. van de Sanden, W. M. M. Kessels, Physica Status Solidi-Rapid Research Letters 2010, 4, 10.

[7] F. Werner, B. Veith, D. Zielke, L. Kuhnemund, C. Tegenkamp, M. Seibt, R. Brendel, J. Schmidt, J. Appl. Phys. 2011, 109, 13701.

[8] J. Frascaroli, G. Seguini, E. Cianci, D. Saynova, J. van Roosmalen, M. Perego, Phys. Status Solidi A 2013, 1-5, DOI: 10.1002/pssa.201200568.

[9] Nicollian E.H, Brews J.R, Metal Oxide Semiconductor Physics and Technology, Wiley, New York 1982.

[10] A. Cuevas, R. A. Sinton, M. Kerr, D. Macdonald, H. Mackel, Solar Energy Materials and Solar Cells 2002, 71, 295.

[11] V. Naumann, M. Otto, R. B. Wehrspohn, C. Hagendorf, Journal of Vacuum Science & Technology A 2012, 30, D4106.

[12] B. Shin, J. R. Weber, R. D. Long, P. K. Hurley, C. G. Van de Walle, P. C. McIntyre, Applied Physics Letters 2010, 96, 52908.

[13] J. R. Weber, A. Janotti, C. G. Van de Walle, J. Appl. Phys. 2011, 109, 33715.

[14] K. Kimoto, Y. Matsui, T. Nabatame, T. Yasuda, T. Mizoguchi, I. Tanaka, A. Toriumi, Applied Physics Letters 2003, 83, 4306.

[15] G. Agostinelli, A. Delabie, P. Vitanov, Z. Alexieva, H. F. W. Dekkers, S. De Wolf, G. Beaucarne, Solar Energy Materials and Solar Cells 2006, 90, 3438.

[16] R. S. Johnson, G. Lucovsky, I. Baumvol, Journal of Vacuum Science & Technology A 2001, 19, 1353.

[17] G. Dingemans, N. M. Terlinden, M. A. Verheijen, M. C. M. van de Sanden, W. M. M. Kessels, J. Appl. Phys. 2011, 110, 93715.

[18] B. Hoex, J. J. H. Gielis, M. C. M. V. de Sanden, W. M. M. Kessels, J. Appl. Phys. 2008, 104, 13703.

[19] S. Steingrube, P. P. Altermatt, D. S. Steingrube, J. Schmidt, R. Brendel, J. Appl. Phys. 2010, 108, 014506.

[20] F. Werner, A. Cosceev, J. Schmidt, J. Appl. Phys. 2012, 111, 073710.

[21] R. N. Hall, Phys. Rev. B 1952, 87, 387.

[22] W. Shockley, W. T. Read, Phys. Rev. B 1952, 87, 835.

[23] S. Dauwe, Thesis, in , Universität Hannover 2004.

[24] Atlas, www.silvaco.com, 2013.